AIAA JOURNAL
Vol. 44, No. 2, February 2006

# Technical Notes

*TECHNICAL NOTES are short manuscripts describing new developments or important results of a preliminary nature. These Notes should not exceed 2500 words (where a figure or table counts as 200 words). Following informal review by the Editors, they may be published within a few months of the date of receipt. Style requirements are the same as for regular contributions (see inside back cover).*

## Nonreflecting Zonal Characteristic Boundary Condition for Direct Numerical Simulation of Aerodynamic Sound

Richard D. Sandberg* and Neil D. Sandham†
*University of Southampton, Southampton, England SO17 1BJ, United Kingdom*

### I. Introduction

SOLVING the full unsteady Navier–Stokes equations to compute directly aerodynamically generated sound has become increasingly feasible due to the dramatic growth in computing power. Both the far-field sound and the near-field hydrodynamics can be predicted, providing an insight into the physical mechanisms of sound generation and potentially helping to validate acoustic theories. One of the problems associated with direct simulations of aerodynamic sound is the large ratio between the energy of the acoustic and the hydrodynamic fields. Under the assumption that a numerical algorithm is in place that can accurately resolve the acoustic field, particular care has to be applied to the boundary conditions to avoid reflections that can potentially render the simulation useless.

Nonreflecting boundary conditions have been extensively studied. In most cases, the boundary conditions are based on characteristic wave analysis and are derived by linearizing the Euler or Navier–Stokes equations.[1–6] This type of local characteristic boundary condition (CBC) has been scrutinized extensively in the literature.[5,7–10] The common conclusion is that the local CBC works satisfactorily for small-amplitude waves, unless the waves are oblique with respect to the respective boundary.[2,4,10] In addition, for flows in which nonlinear disturbances, such as high-energy vortical structures in shear or jet flows, cross the outflow boundary, considerable acoustic reflections are generated by the local CBC. For simulations, where it is essential that the high-energy structures exit the computational domain with minimal acoustic reflections, it was found necessary to add nonphysical buffer zones to the physical domain. Colonius et al.[8] combined grid stretching with low-pass filtering to reduce spurious oscillations produced by the coarsening grid. Other zonal approaches include adding a dissipation term to the right-hand side (RHS) of the governing equations, forcing the flow solution to a target state,[11,12] or adding a convection term to the RHS to achieve supersonic flow at the outflow boundary.[13] These two methods have also been combined for in- and outflow boundary conditions and have been shown to be highly effective.[10] However, such approaches involve coefficients that are highly flow dependent and assume prior knowledge of the size of the structures to be damped. In the current Note, traditional characteristic boundary conditions are extended to a highly effective zonal approach that does not include any additional constants.

Received 28 July 2005; revision received 23 September 2005; accepted for publication 6 October 2005. 

*Research Fellow, School of Engineering Sciences; sandberg@soton.ac.uk. Member AIAA.
†Professor, School of Engineering Sciences; n.sandham@soton.ac.uk. Member AIAA.

### II. Zonal Characteristic Boundary Condition

Characteristic analysis[2] is used to modify the hyperbolic terms of the compressible Navier–Stokes equations corresponding to waves propagating in the direction normal to a boundary. The amplitude of characteristic waves $\mathcal{L}_i$ associated with characteristic velocities $\lambda_i$, with $i = 1, \ldots, 5$, are obtained. Based on the sign of the eigenvalues $\lambda_i$, which determine whether the acoustic, vorticity, or entropy waves are incoming or outgoing, $\mathcal{L}_i$ are specified or left untreated at the respective boundary. For a subsonic outflow boundary, four characteristics are outgoing and the characteristic associated with $\lambda_1 = u - c$ is incoming, where $u$ is the streamwise velocity component and $c$ is the speed of sound. In case the flow is not a straight duct, the outflow direction is considered to be normal to the outflow boundary. Commonly, the amplitude of the rate of change of the characteristic wave $\mathcal{L}_1$ at the boundary is either set to zero[2,5] or as $\mathcal{L}_1 = K(p - p_\infty)$ to ensure a well-posed nature, adding an additional constant $K$ (Refs. 7 and 14). Here, the treatment of $\mathcal{L}_1$ is not restricted to the boundary itself, but is applied within a zone. The eigenvalues $\lambda_i$ and the associated eigenvectors $\mathcal{L}_i$ are computed within a specified buffer zone and left unchanged when $\lambda_i \geq 0$ within this region. For $\lambda_i < 0$, the amplitude of the characteristic wave is gradually ramped to zero at the outflow according to

$$\tilde{\mathcal{L}}_i = g(x) \cdot \mathcal{L}_i, \qquad g(x) = 0.5\left\{1 + \cos\left[\frac{\pi(x - x_s)}{(x_{\text{out}} - x_s)}\right]\right\} \tag{1}$$

where $x_s$ is the onset of the buffer zone and $x_{\text{out}}$ denotes the outflow boundary. This approach is easily extended to local one-dimensional inviscid (LODI)[7] relations, which are commonly used when solving the full Navier–Stokes equations. The modified wave amplitude variations $\tilde{\mathcal{L}}_i$ are used to assemble the gradients normal to the boundaries. The extension to boundaries other than the outflow is straightforward, treating $\mathcal{L}_i$ as desired, albeit multiplying by a ramping function within a zone instead of modifying $\mathcal{L}_i$ only at the boundary itself. Here, for brevity, the performance of the proposed method is demonstrated only for the outflow boundary.

### III. Analysis

A two-dimensional compressible vortex in a uniform flow is considered.[15] The length-, velocity- and timescales are $\Delta x = \Delta y$, $U_\infty$ (speed of uniform flow) and $\Delta x / U_\infty$, respectively. The reference density is $\rho_\infty$, and the reference pressure is $\rho_\infty U_\infty^2$. As an initial condition, the non-dimensional velocity components in the $x$ and $y$ direction are specified as

$$u_0 = 1 + \epsilon y \exp\left[-\ell n 2(x^2 + y^2)/r_v\right]$$

$$v_0 = -\epsilon x \exp\left[-\ell n 2(x^2 + y^2)/r_v\right] \tag{2}$$

respectively, with the vortex strength $\varepsilon = 0.03/M$, the Mach number $M$, and the radius $r_v = 5$. Both initial density and temperature

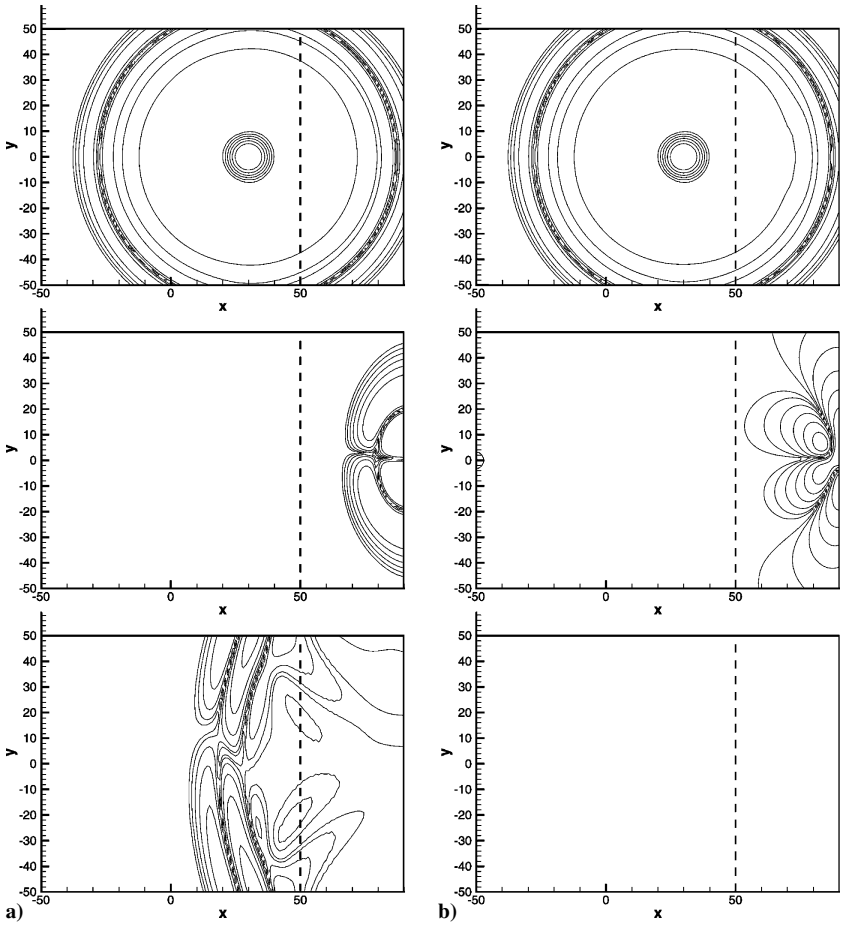


**Fig. 1 Contours of normalized disturbance pressure for single vortex problem with buffer zone using a) local CBC and b) zonal CBC at, from top to bottom, $t = 30$, 100, and 160; six exponentially distributed contour levels for [0.002; 0.064].**

are set to unity, and the initial pressure follows as $p_0 = 1/(\gamma M^2)$. Specifying uniform density and pressure fields instead of accounting for the distribution caused by the vortex is intended to generate an initial acoustic pulse. Hence, the performance of the zonal CBC with respect to sound waves can be evaluated. The Mach number was set to $M = 0.5$ and the global Reynolds number to $Re = 1 \times 10^5$ to minimize the influence of viscosity. The physical domain has the dimensions $-50 \leq x, y \leq 50$ and is discretized with $N_x = N_y = 101$ uniform grid points in each direction. To absorb the sound waves caused by the acoustic pulse, sponge zones are placed at $-70 \leq x < -50$ and $50 < |y| \leq 70$, which are kept fixed for all simulations. At the outflow, a buffer zone with 40 uniformly spaced grid points in $50 < x \leq 90$ is specified in which the following techniques were applied: using a local CBC, the zonal CBC, or employing a sponge layer with a local CBC. Three variants of sponge layers were investigated, 1) a procedure that directly forces the solution to a target within the sponge zone, requiring a coefficient $\sigma(x)$; 2) a dissipation term added to the RHS of the governing equations, also requiring a constant $\sigma(x)$[11]; and 3) a dissipation term and a convective term added to the RHS[10] using the coefficients $\sigma(x)$ and $U_c(x)$, respectively. Numerous coefficients and ramping functions were explored, and only the most successful combinations are discussed here: $\sigma(x) = 0.05[1 - g(x)]$ and $U_c(x) = 0.5[1 - g(x)]$, where $g(x)$ is given according to Eq. (1). Visualizations of vorticity showed that using just the local CBC is satisfactory for the hydrodynamic field, permitting the vortex to exit the computational domain smoothly. However, to show the inadequacy of the local CBC for the acoustic field, contours of normalized disturbance pressure $|(p(x, y) - p_0)M^2/\epsilon|$ (dashed line denotes onset of the buffer zone) are shown for three time instants in Fig. 1. The images at $t = 30$ illustrate that the sound wave originating from the acoustic pulse is not affected by the zonal CBC but travels through the buffer zone without being modified, in contrast with all other sponge techniques investigated in this study. It is also apparent that no visible reflections are caused by the local CBC for this kind of perturbation. At $t = 100$, however, just after the center of the single vortex crosses the outflow boundary ($t = 90$), the generation of considerable acoustic waves at the outflow boundary can be observed in the local CBC case. At $t = 160$, these reflected spurious pressure waves contaminate a large portion of the physical domain. When the zonal CBC is employed, the single vortex is severely altered within the buffer zone causing spurious pressure oscillations. However, here these waves are not permitted to travel upstream because the incoming characteristics are slowly ramped to zero over the entire buffer zone. At $t = 160$, no pressure oscillations are visible in both the physical domain and the buffer zone. This qualitatively illustrates the benefit of using the zonal CBC.

To assess more quantitatively the magnitude of the reflected pressure waves into the physical domain, the norm of the residual disturbance pressure $L_p$ is computed according to

$$L_p = \left\{ \frac{1}{N_x N_y} \sum_{x,y}^{N_x, N_y} [p(x, y) - p_0]^2 \right\}^{\frac{1}{2}} \tag{3}$$

Figure 2 shows the results obtained for various methods. For all cases, $L_p$ rises to approximately $2 \times 10^{-3}$ initially and slowly decays in time (due to viscosity), whereas the vortex moves toward the outflow boundary. For a case where no buffer zone was employed, albeit using a local CBC, strong reflections from the outflow boundary cause $L_p$ to increase considerably for $t > 40$ before slowly recovering to marginally lower levels. When a buffer zone is added with the local CBC at the outflow, $L_p$ decays rapidly once the vortex leaves the physical domain. However, as seen in Fig. 1, considerable reflections are caused when the vortex reaches the outflow boundary ($t = 90$), which propagate upstream and lead to an increase in $L_p$

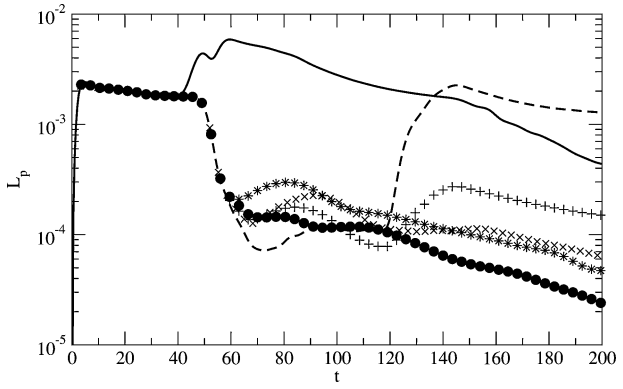


**Fig. 2 Residual pressure $L_p$ in physical domain: —, no buffer zone; – –, buffer zone with local CBC; ∗, method 1; +, method 2; ×, method 3; and •, zonal CBC.**

once they have reached the physical domain ($t > 120$). In fact, $L_p$ rises to a level even higher than in the case without a buffer zone. Employing method 1 achieves a considerable reduction of $L_p$. $L_p$ was reduced further initially in case 2, however, once the reflections from the outflow boundary reach the physical domain, $L_p$ attains a fairly large level. Method 3 improves the performance of the buffer zone in that the increase in $L_p$ further in time is reduced. Using the zonal CBC results in the best overall performance, in particular for $t > 120$, at which all other methods show an increase of $L_p$ due to reflections from the outflow boundary reaching the physical domain. That the $L_p$ distributions deviate from the case using the local CBC starting at around $t = 58$ for all methods investigated illustrates that any kind of treatment causes reflections by itself within the buffer zone. For the cases presented, these were already minimized by the choice of a ramping function with a smooth onset.

The simulations were repeated with other buffer zones. Results obtained when using a buffer zone with 20 nonuniformly spaced grid points in $50 < x \leq 90$ were similar to the data shown earlier, implying that the grid stretching did not contribute considerably to damping reflections. It is, rather, the physical length of the buffer zone that has a significant effect on the performance of all techniques investigated here, evidenced by inferior results obtained using a buffer zone with 20 uniformly spaced grid points in $50 < x \leq 70$. However, even for the shortest buffer zone, the zonal CBC was superior to all other methods tested.

## IV. Trailing-Edge Simulation

After completion of initial testing with model problems, the proposed zonal CBC was employed for direct numerical simulation of compressible flow over a singular plate with a trailing edge (TE). The aim of these simulations is to evaluate the acoustic scattering of Tollmien–Schlichting (T–S) waves convecting over the TE. Significantly reducing residual pressure oscillations caused by vortical structures in the wake crossing the outflow boundary is essential for capturing the low-amplitude sound waves produced at the TE. Because of the high computational expense of such simulations, a method was sought that does not require the calibration of coefficients. This, in fact, motivated the development of the proposed zonal CBC. The computational domain has the dimensions $3 \leq x \leq 11$ and $-5 \leq y \leq 5$. The singular plate at $y = 0$ extends from the inflow boundary to $x = 6$. The low-amplitude T–S waves are introduced at $x = 3.25$ with a nondimensional frequency $\omega = 1.1111$. At the TE, the top and bottom boundary layers have a displacement thickness of $\delta^* = 0.0192$, resulting in $Re_{\delta^*} = 960$. There are 1800 and 400 nonequidistantly spaced points used for the $x$ and $y$ directions, respectively, with the finest resolution at the TE. A high-order-accurate full compressible Navier–Stokes solver employing entropy splitting for the convective terms[16] is used for the simulations at $M = 0.6$. In Fig. 3, isocontours of the magnitude of dilatation are shown of the flowfield after nine flow-through times. The dashed line denotes the onset of a region employing low-pass filtering, along with strong grid stretching,[8] which accounts for merely 5.5% of the streamwise points.

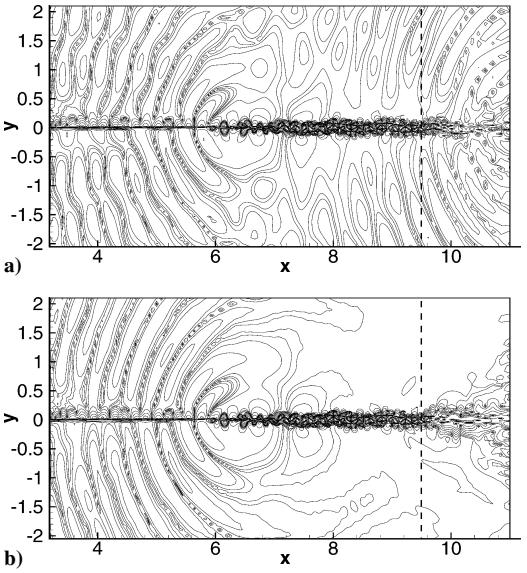


**Fig. 3 Contours of magnitude of dilatation for TE simulations a) using a local CBC combined with low-pass filtering and strong grid-stretching and b) using the zonal CBC; eight exponentially distributed contour levels for [0.0005; 0.064]; $Re = 5 \times 10^4$ and $M = 0.6$.**

This region achieves a considerable reduction of vorticity magnitude of the structures. Nevertheless, when using the local CBC, severe acoustic reflections can be observed that propagate upstream and contaminate the region of interest. These reflections clearly interact with the low-amplitude sound waves scattered from the TE. In contrast, when the zonal CBC is employed using the ramping function $g(x)$ given by Eq. (1) within the buffer region, the results are dramatically improved. This is particularly encouraging because the scheme was transferred from the test-problem described earlier with no further modification. The computational cost of using the zonal CBC over a local CBC increased by roughly 6% in the preceding case. Hence, the proposed zonal CBC appears to offer a coefficient-free and inexpensive way of drastically reducing spurious pressure oscillations.

## V. Conclusions

A nonreflecting zonal boundary condition was presented. The method is based on commonly used characteristic boundary conditions and, therefore, only requires marginal modifications to existing codes. Here, incoming characteristics are ramped to zero in a buffer zone as opposed merely to setting them to zero at the boundary. Crucially, in contrast to most other zonal approaches, the method is free of coefficients that require calibration. It is shown that the proposed zonal boundary condition succeeds in significantly reducing spurious pressure oscillations that are produced when vortical structures in compressible flows cross the far-field boundaries.

## Acknowledgments

This work was supported by the Department of Trade and Industry under the Modelling and Simulation of Turbulence and Transition in Aerospace Defence and Aerospace Research Partnership program. Computer time was partly provided by Engineering and Physical Sciences Research Council Grant GR/S27474/01.

## References

[1]Enquist, B., and Majda, A., "Absorbing Boundary Condition for the Numerical Simulation of Waves," *Mathematics of Computation*, Vol. 31, No. 139, 1977, pp. 629–651.

[2]Thompson, K. W., "Time Dependent Boundary Conditions for Hyperbolic Systems," *Journal of Computational Physics*, Vol. 68, 1987, pp. 1–24.

[3]Gustafsson, B., "Far-Field Boundary Conditions for Time-Dependent Hyperbolic Systems," *SIAM Journal of Scientific and Statistical Computing*, Vol. 9, No. 5, 1988, pp. 812–828.

[4]Giles, M., "Nonreflecting Boundary Conditions for Euler Equations Calculations," *AIAA Journal*, Vol. 18, No. 12, 1990, pp. 2050–2058.

[5]Hayder, M., and Turkel, E., "Nonreflecting Boundary Conditions for Jet Flow Computations," *AIAA Journal*, Vol. 33, No. 12, 1995, pp. 2264–2270.

[6]Tam, C., and Dong, Z., "Radiation and Outflow Boundary Conditions for Direct Computation of Acoustic and Flow Disturbances in a Nonuniform Mean Flow," *Journal of Computational Acoustics*, Vol. 4, No. 2, 1996, pp. 175–201.

[7]Poinsot, T. J., and Lele, S. K., "Boundary Conditions for Direct Simulations of Compressible Viscous Flows," *Journal of Computational Physics*, Vol. 101, No. 1, July 1992, pp. 104–129.

[8]Colonius, T., Lele, S. K., and Moin, P., "Boundary Conditions for Direct Computation of Aerodynamic Sound Generation," *AIAA Journal*, Vol. 31, No. 9, 1993, pp. 1574–1582.

[9]Atkins, H., and Casper, J., "Nonreflective Boundary Conditions for High-Order Methods," *AIAA Journal*, Vol. 32, No. 3, 1994, pp. 512–518.

[10]Freund, J., "Proposed Inflow/Outflow Boundary Condition for Direct Computation of Aerodynamic Sound," *AIAA Journal*, Vol. 35, No. 4, 1997, pp. 740–742.

[11]Berenger, J., "A Perfectly Matched Layer for the Absorption of Electromagnetic Waves," *Journal of Computational Physics*, Vol. 114, No. 2, 1994, pp. 185–200.

[12]Hu, F. Q., "On Absorbing Boundary Conditions for Linearized Euler Equations by a Perfectly Matched Layer," *Journal of Computational Physics*, Vol. 129, 1996, pp. 201–219.

[13]Tas'an, S., and Nark, D., "An Absorbing Buffer Zone Technique for Acoustic Wave Propagation," AIAA Paper 95-0146, 1995.

[14]Kim, J., and Lee, D., "Generalized Characteristic Boundary Conditions for Computational Aeroacoustics," *AIAA Journal*, Vol. 38, No. 11, 2000, pp. 2040–2049.

[15]Hardin, J., Ristorcelli, J., and Tam, C., "Workshop on Benchmark Problems in Computational Aeroacoustics," NASA CP 3300, Oct. 1995.

[16]Sandham, N., Li, Q., and Yee, H., "Entropy Splitting for High-Order Numerical Simulation of Compressible Turbulence," *Journal of Computational Physics*, Vol. 178, No. 2, 2002, pp. 307–322.

D. Gaitonde
*Associate Editor*